Structural insights into the mechanism of the sodium/iodide symporter (NIS)

Silvia Ravera[1], Juan Pablo Nicola[2], Glicella Salazar de Simone[3], Fred J. Sigworth[4], Erkan Karakas[1], L. Mario Amzel[5#], Mario A. Bianchet[6], and Nancy Carrasco[1&*]

[1] Department of Molecular Physiology and Biophysics, Vanderbilt University, Nashville, TN 37232, USA,
[2] Department of Clinical Biochemistry, National University of Córdoba, Córdoba, Argentina,
[3] Department of Obstetrics and Gynecology, Columbia University Medical Center, New York, NY 10032, USA,
[4] Department of Cellular and Molecular Physiology, Yale School of Medicine, New Haven, CT 06510, USA,
[5] Department of Biophysics and Biophysical Chemistry, Johns Hopkins University School of Medicine, Baltimore, MD 21205, USA, and
[6] Department of Neurology, Johns Hopkins University School of Medicine, Baltimore, MD 21205, USA.

[#] L.M.A. passed away on August 28, 2021.
[*]Correspondence and requests for materials should be addressed to N.C. (email: nancy.carrasco@vanderbilt.edu)

This file contains Supplementary Figures 1-11 and Supplementary Table 1.

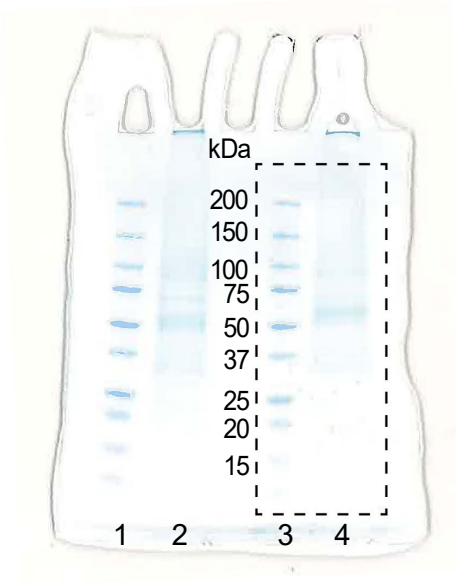

Supplementary Fig. 1 | Electrophoretic pattern of purified NIS. Lanes 1 and 3: molecular weight markers; lane 2: NIS after affinity purification; lane 4: NIS after size exclusion chromatography. The gel was stained with Coomassie Blue. Dotted rectangle is shown in Extended Data Fig.1.

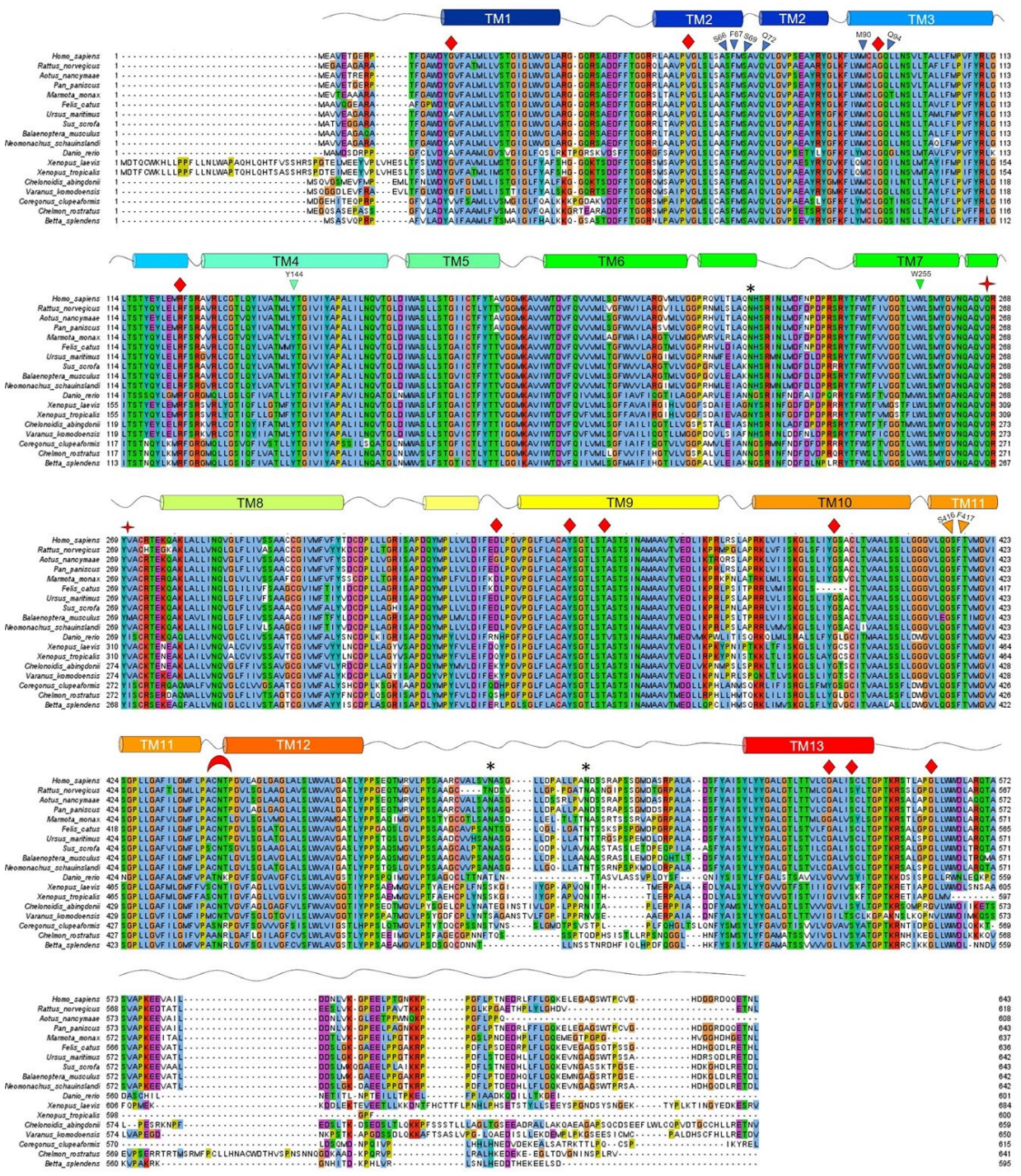

Supplementary Fig. 2 Alignment of NIS sequences from different species. α-helices are represented by cylinders. Glycosylation sites are marked with a *; critical residues with inverted triangles; non-WT residues found in IDD patients with diamonds; and the deletion Δ439-443 found in IDD patients with a crescent moon. The alignment was done using Clustaw Omega and displayed using Jalview.

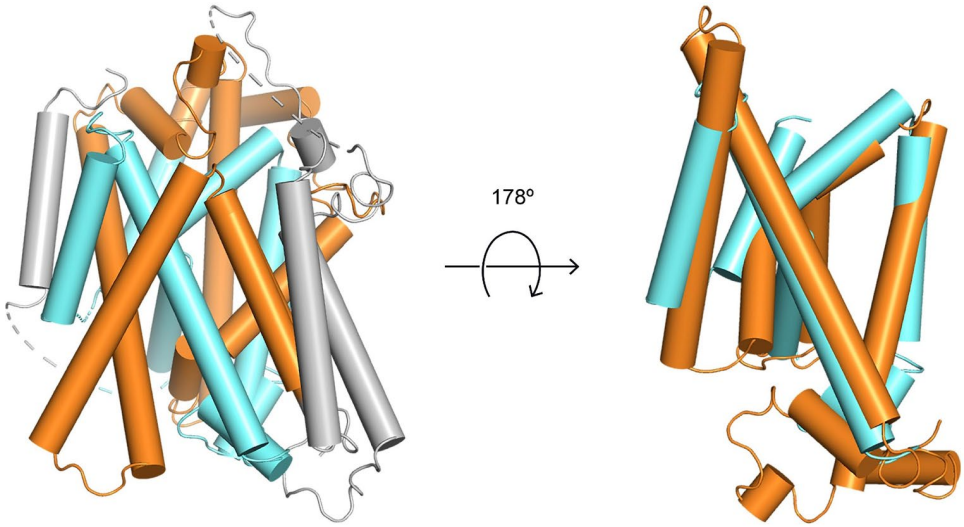

Supplementary Fig. 3 |Alignment of the inverted structural repeats. NIS has a LeuT fold with two 5-helix bundle domains (TMSs 2-6 and 7-11) related by a pseudo-two-fold symmetry. The alignment between the two repeats shows a root mean square deviation (RMSD) of 3.0 Å.

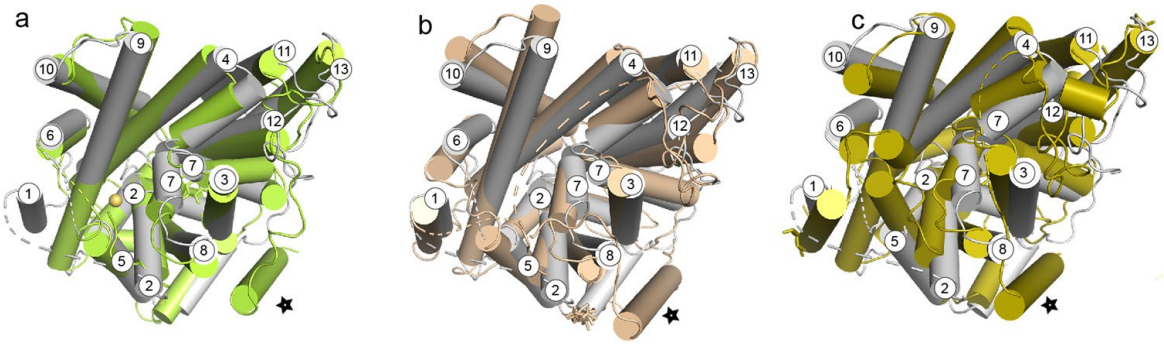

Supplementary Fig. 4 | Structural alignment between NIS in grey, vSGLT (pdb accession code 3DH4) in green (a), hSGLT1 (pdb accession code 7SLA) in wheat (b), and hSGLT2 (pdb accession code 7VSI) in olive (c). *the stars in g, h, and i indicate the extra TMSs present in vSGLT, hSGLT1, and hSGLT2.

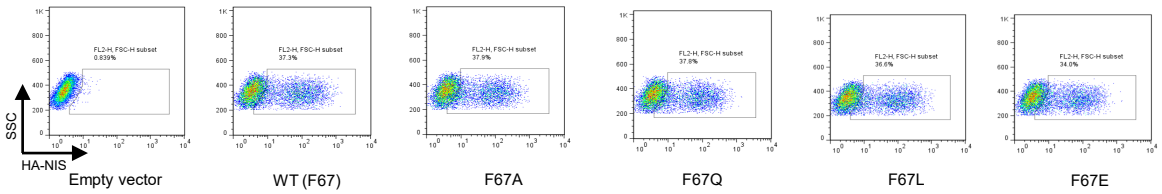
SSC
HA-NIS
Empty vector
WT (F67)
F67A
F67Q
F67L
F67E
F67K
F67H

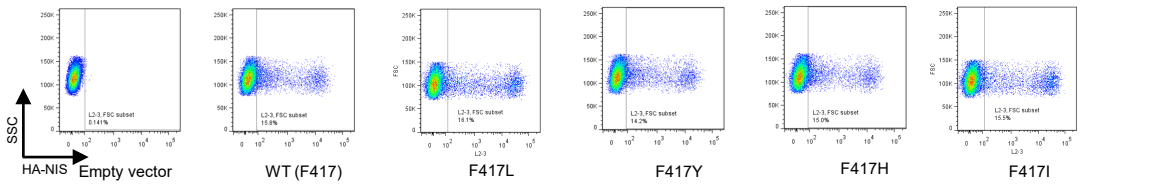
SSC
HA-NIS
Empty vector
WT (F417)
F417L
F417Y
F417H
F417I

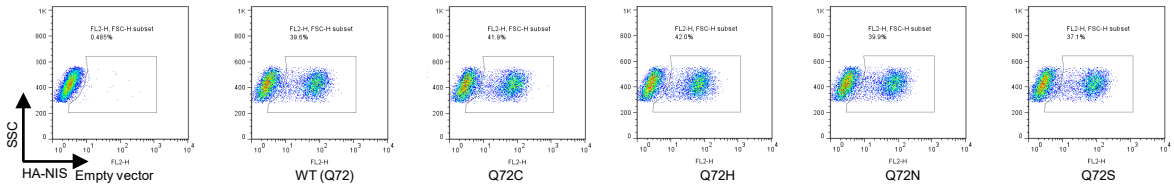
SSC
HA-NIS
Empty vector
WT (Q72)
Q72C
Q72H
Q72N
Q72S

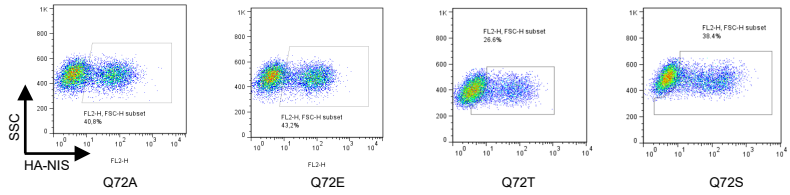
SSC
HA-NIS
Q72A
Q72E
Q72T
Q72S

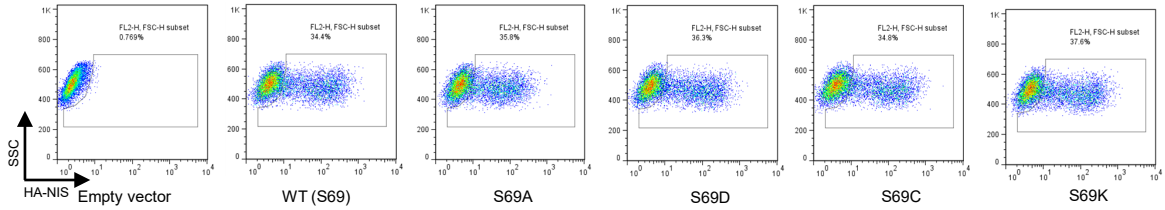
SSC
HA-NIS
Empty vector
WT (S69)
S69A
S69D
S69C
S69K

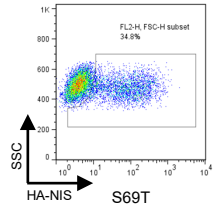
SSC
HA-NIS
S69T

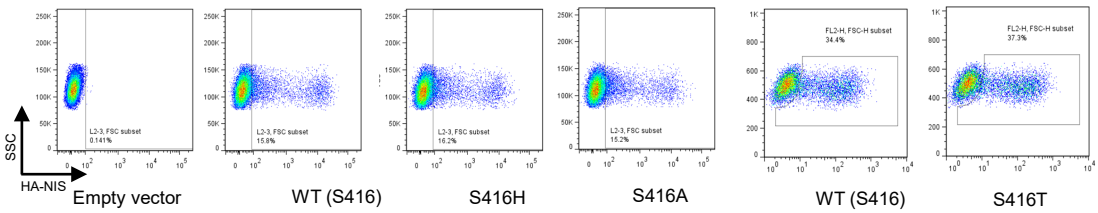
SSC
HA-NIS
Empty vector
WT (S416)
S416H
S416A
WT (S416)
S416T

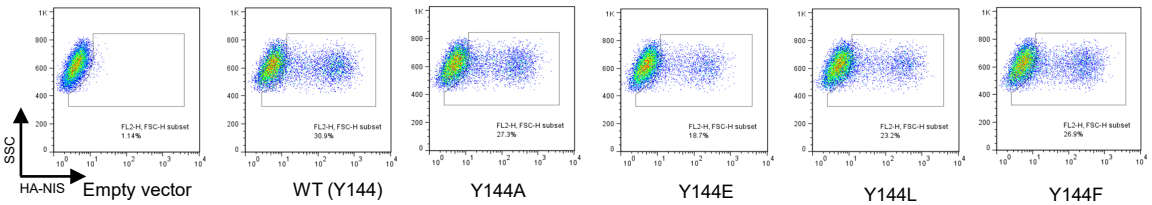
SSC
HA-NIS
Empty vector
WT (Y144)
Y144A
Y144E
Y144L
Y144F

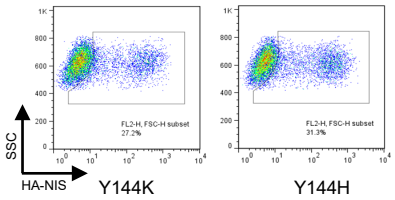
SSC
HA-NIS
Y144K
Y144H

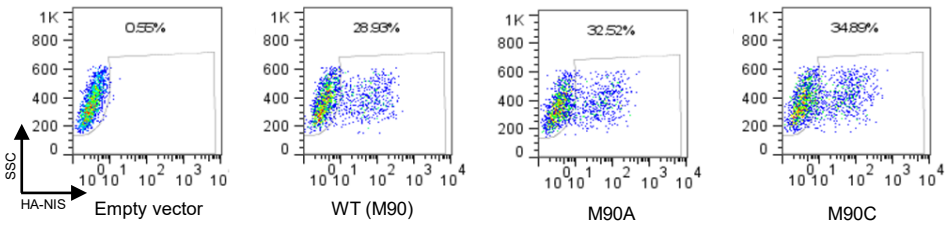
0.55%
28.98%
32.52%
34.89%
SSC
HA-NIS
Empty vector
WT (M90)
M90A
M90C

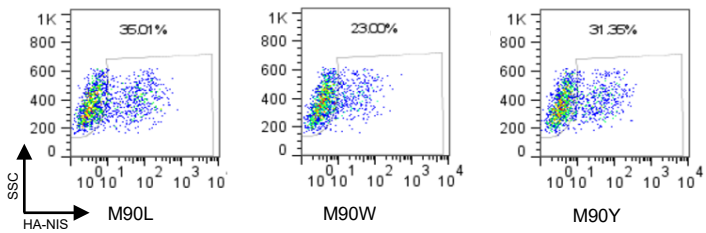
35.01%
23.00%
31.36%
SSC
HA-NIS
M90L
M90W
M90Y

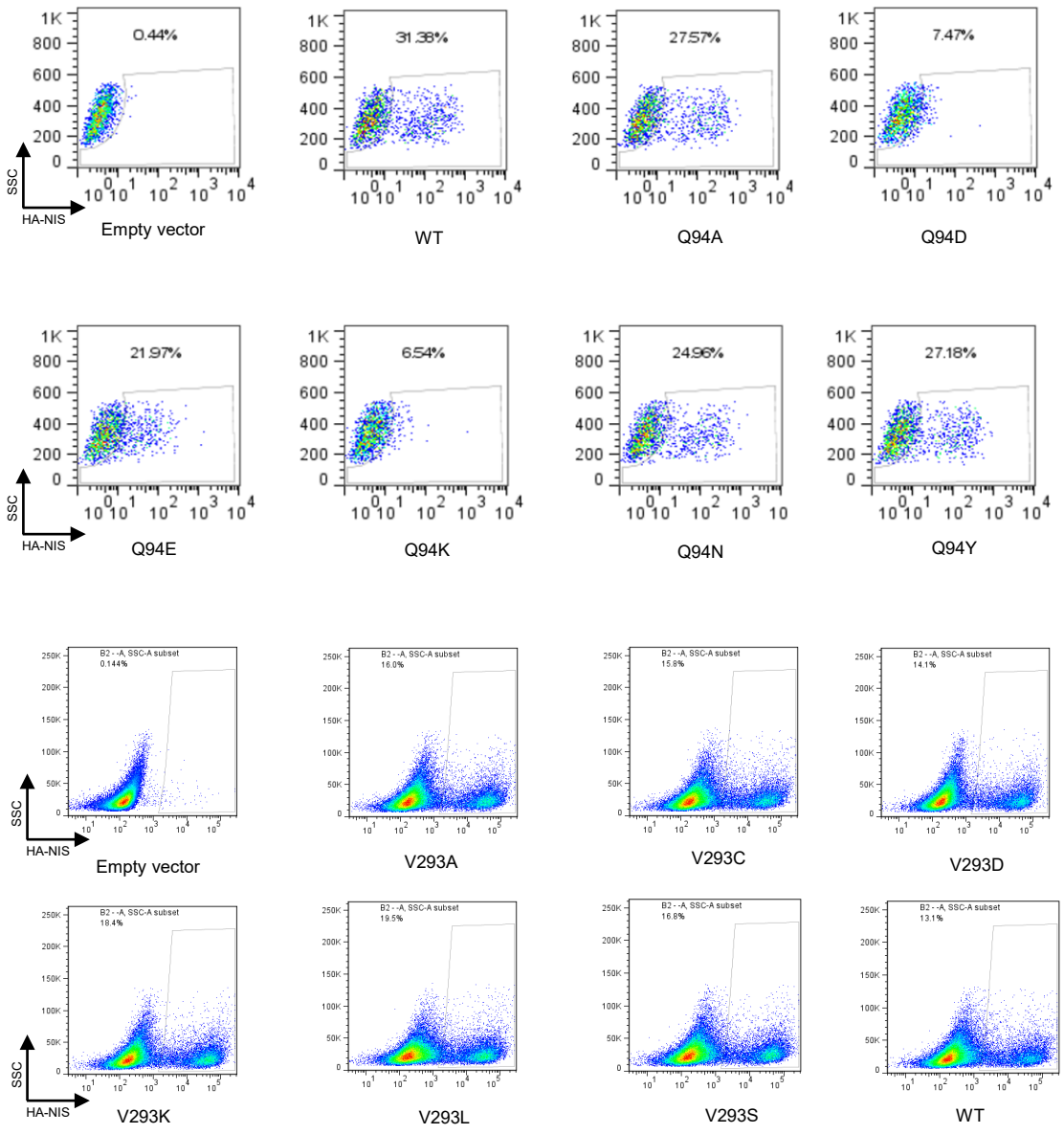

Supplementary Fig. 5 NIS mutant proteins are properly targeted to the plasma membrane. HEK cells transfected with an empty plasmid (i.e., not containing the cDNA of interest) and HEK cells transfected with WT NIS or the indicated NIS mutants were incubated under nonpermeabilized conditions with an anti-HA antibody that recognizes the extracellular N-terminus HA epitope and analyzed by flow cytometry. The x axes show the intensity of the fluorescence of each single cell; the y axes the values of the side scatter parameters. For each experiment, cells transfected with an empty plasmid were used as a reference to identify the negative cells and determine the percentage of cells expressing WT NIS or the respective mutants.

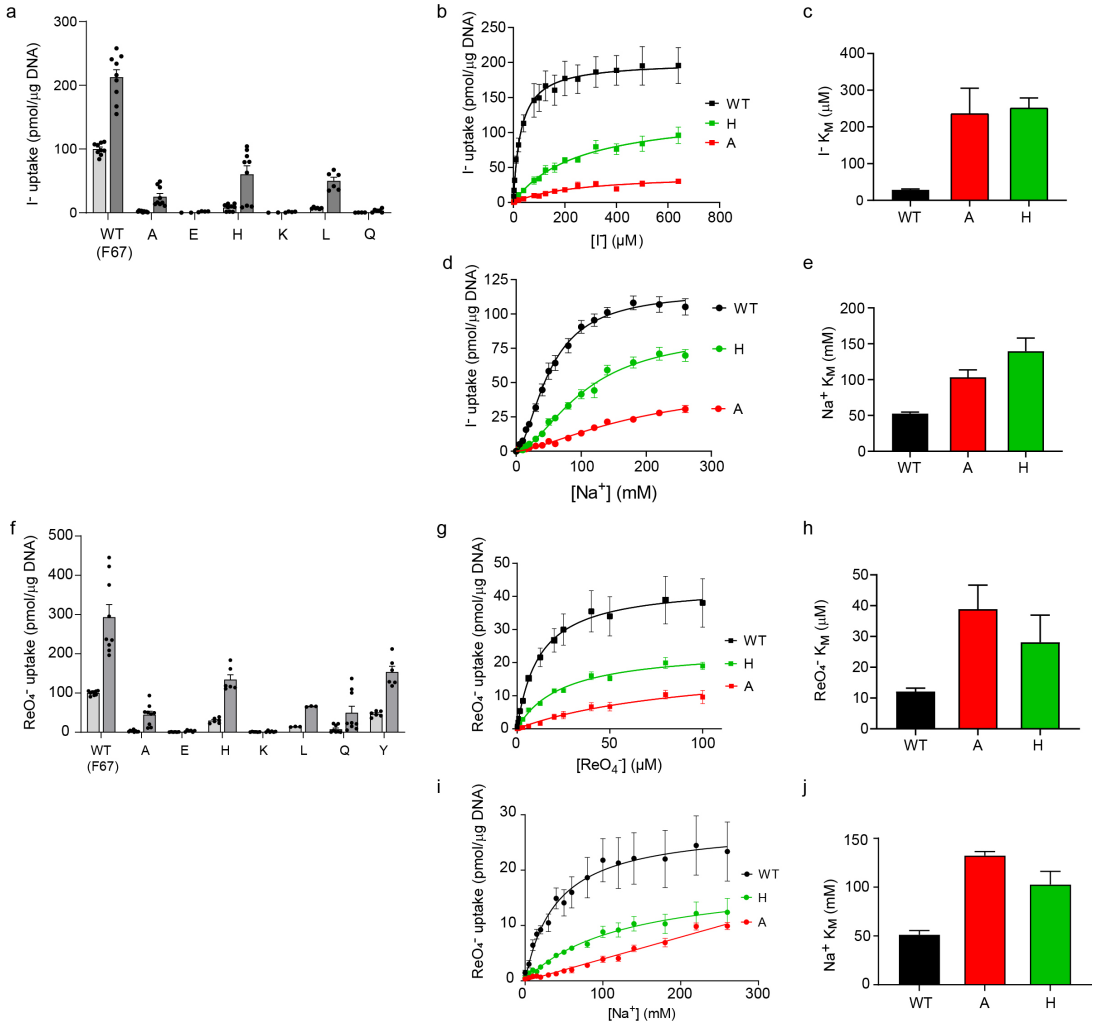

Supplementary Fig. 6 Effect of single amino acid substitutions at position 67 on I^- and ReO_4^- transport. a. NIS-mediated I^- uptake at steady state. cDNA constructs coding for NIS mutants in which F67 is replaced with the residues indicated were transfected into COS7 or HEK cells. I^- uptake by these NIS mutants was measured at 20 µM (white bars) and 200 µM (gray bars) I^- at 140 mM Na^+ for 30 min with or without the NIS-specific inhibitor ClO_4^- (values obtained in the presence of ClO_4^-, which are < 10% of the values obtained in its absence, have already been subtracted). Results are given as pmols of I^- accumulated/µg DNA ± s.e.m. Values represent averages of the results from two or three different experiments, each of which was carried out in triplicate (n = 6-9). **b and d**. Kinetic analysis of initial rates of I^- uptake (2-min time points) determined at 140 mM Na^+ and varying concentrations of I^- (b), and at varying concentrations of Na^+ and 500 µM I^- (d). **c and e.** I^- K_M and Na^+ K_M values determined from b and d, respectively. The error bars represent the standard deviation of the Michaelis Menten (b), and Hill equation (d) analysis. **f.** NIS-mediated ReO_4^- uptake at steady state. ReO_4^- uptake by these NIS mutants was measured at 3 µM (white bars) and 30 µM (gray bars) ReO_4^- at 140 mM Na^+ for 30 min with or without the NIS-specific inhibitor ClO_4^- (values obtained in the presence of ClO_4^-, which are < 10% of the values obtained in its absence, have already been subtracted). Results are given as pmols of I^- accumulated/µg DNA ± s.e.m. Values represent averages of the results from two or three different experiments, each of which was carried out in triplicate. **g and i**. Kinetic analysis of initial rates of ReO_4^- uptake (2-min time points) determined at 140 mM Na^+ and varying concentrations of ReO_4^- (g), and at varying concentrations of Na^+ and 100 µM ReO_4^- (i). **h and j.** ReO_4^- and Na^+ K_Ms values determined from g and i, respectively. The error bars represent the standard deviation of the Michaelis Menten (g), and Hill equation (i) analysis.

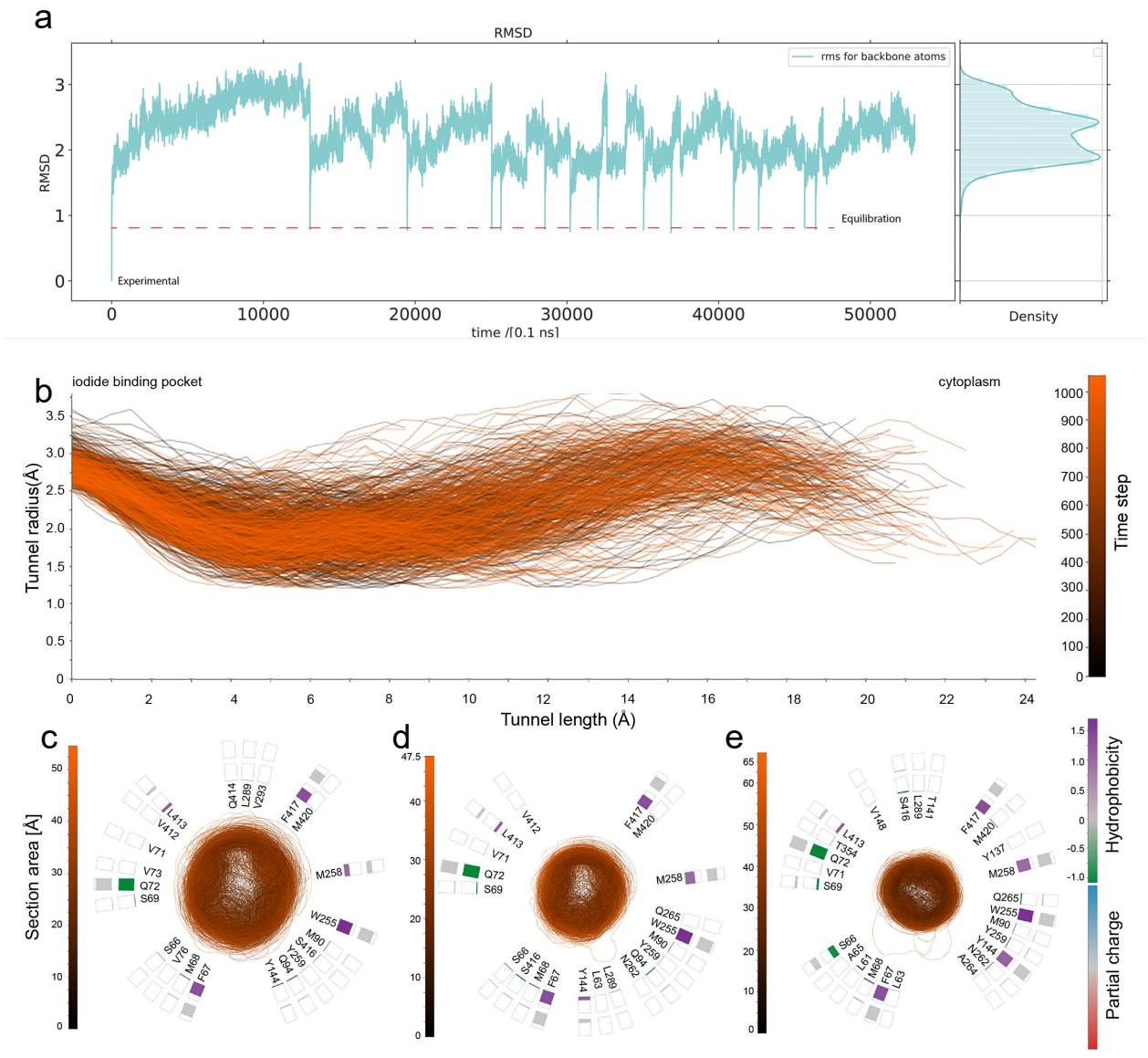

Supplementary Fig. 7 MD simulations. a. RMSD plot of the accumulated trajectories from 13 different MD simulations of various lengths, showing the RMSDs between C-α atoms in the experimental and simulated structures. In each of the thirteen runs, the structure was equilibrated using a different distribution of initial velocities at a temperature of 310.15 K. The red dashed line indicates the approximate starting value of the equilibrate structure used in each leg of the production stage. The time-series plot of the RMSDs clearly shows that they plateaued, indicating that there is no systematic change in the dynamic structure (left panel). Histogram of the RMSD distribution (right panel). **b**. Cluster of tunnels identified in 1059 snapshots from the MD simulations carried out with NIS-I^-. A pathway analysis performed on 1059 snapshots from the MD simulations with the NIS-I- structure sampled every 5 ns revealed a cluster of tunnels similar to the one in the apo-NIS structure in 95 ± 0.03% of the snapshots. The analysis was carried out as follows: the snapshots were divided into 10 groups, the tunnels in each group were counted, and the average of the counts computed with its standard deviation. **c-e.** section of the tunnel cluster taken respectively at 3.5 Å (a), 5 Å (b), and 10 Å (c) from the position of the I^- binding in the structure. We used CAVER Analyst 2.0 (BETA 2) with the default parameters, with the exception of a probe radius of 1.2 (Å), a clustering threshold of 5.3 (Å) , and a shell depth of 5 (Å); the ions were excluded.

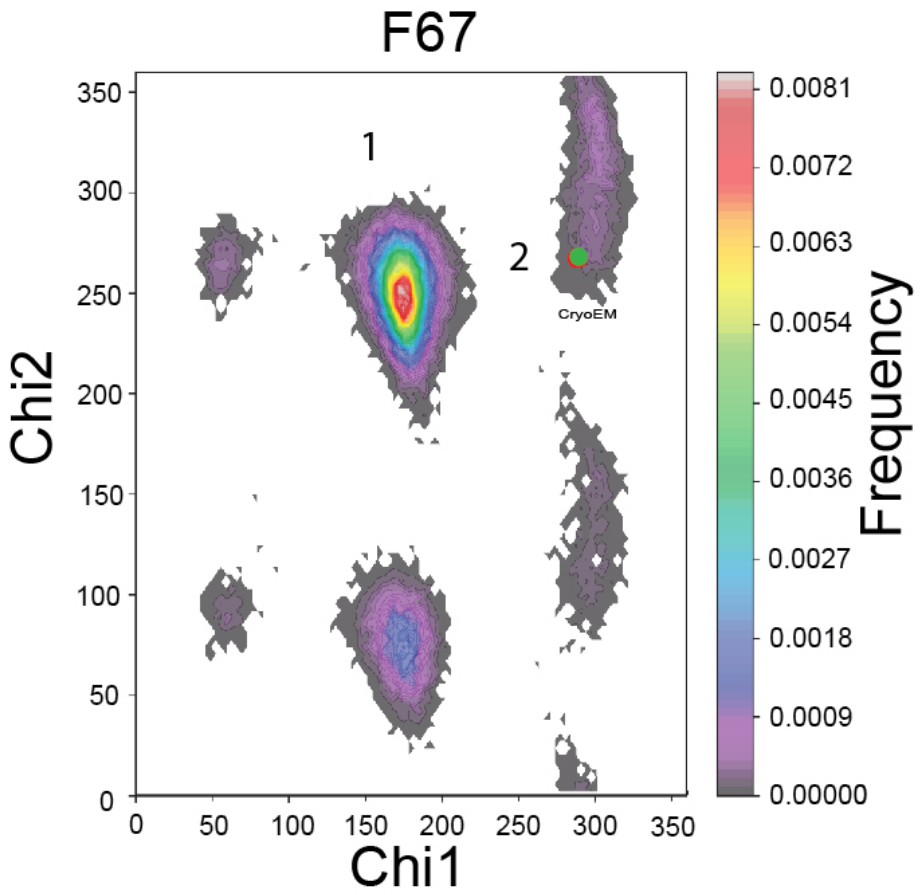

Supplementary Fig. 8 F67 conformations open up the ion pocket toward the exit pathway. Ramachandran plot of the chi1 and chi2 side chain dihedral angles of F67 visited during the MD simulations with NIS-I^-. The dihedral angles selected are the principal determinants of the position of the side chain. The excursions of these dihedral angles (during the MD simulations) away from the conformational basins corresponding to the cryoEM structure (green dot in basin 2) and toward conformational basins (blue dot in basins 1) open up the exit path. In these histograms, the frequency of a given conformational state is indicated by a rainbow gradient from deep purple (0 frequency) to red (highest frequency).

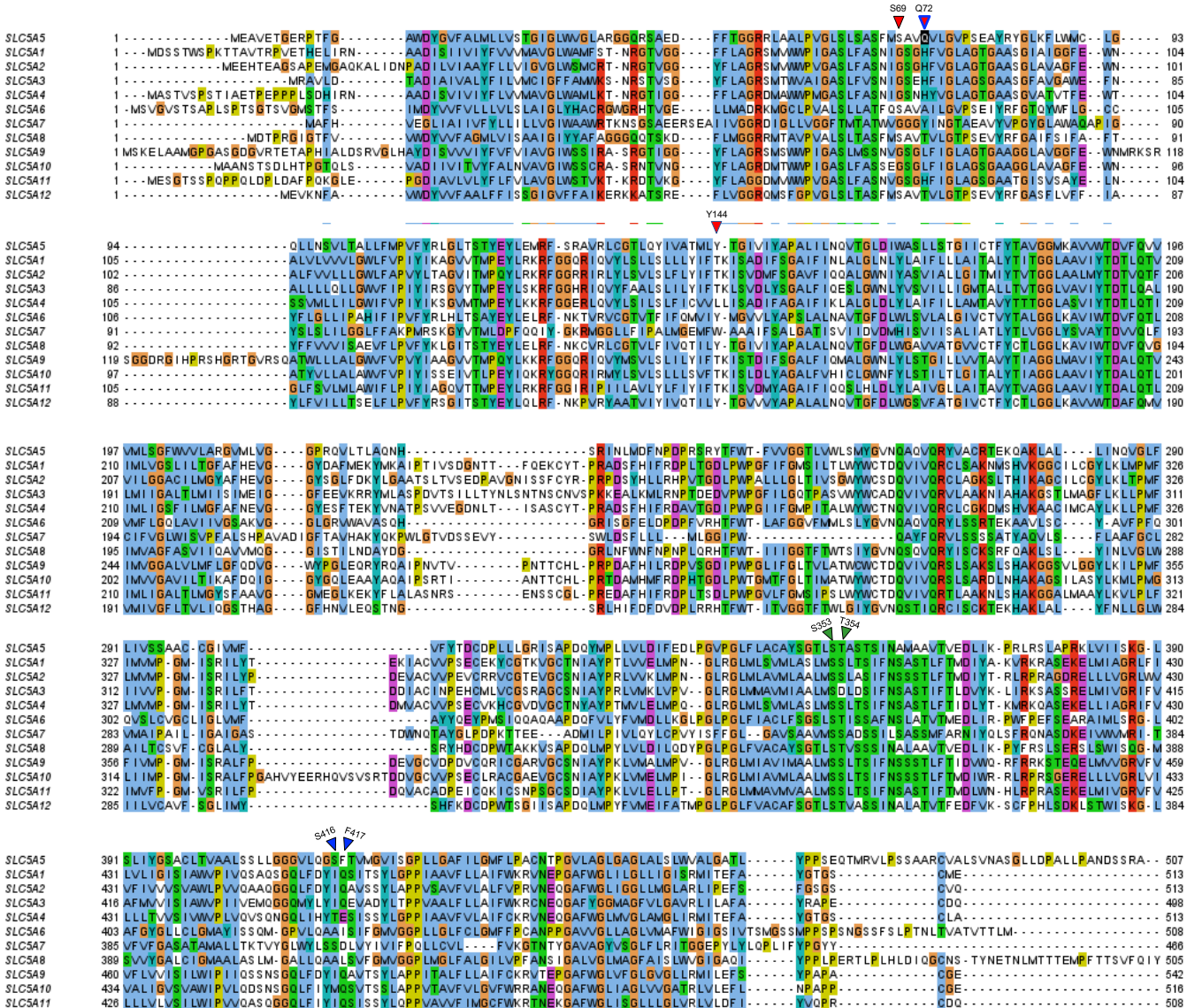

Supplementary Fig. 9 Alignment of the sequences of the members of the SLC5 family. The red inverted triangles indicate the residues interact with Na1; the blue inverted triangles, the residues that interacts with Na2; and the green inverted triangles, the residues whose side chains contribute to forming the canonical Na2 site. The alignment was done using Clustaw Omega and displayed using Jalview.

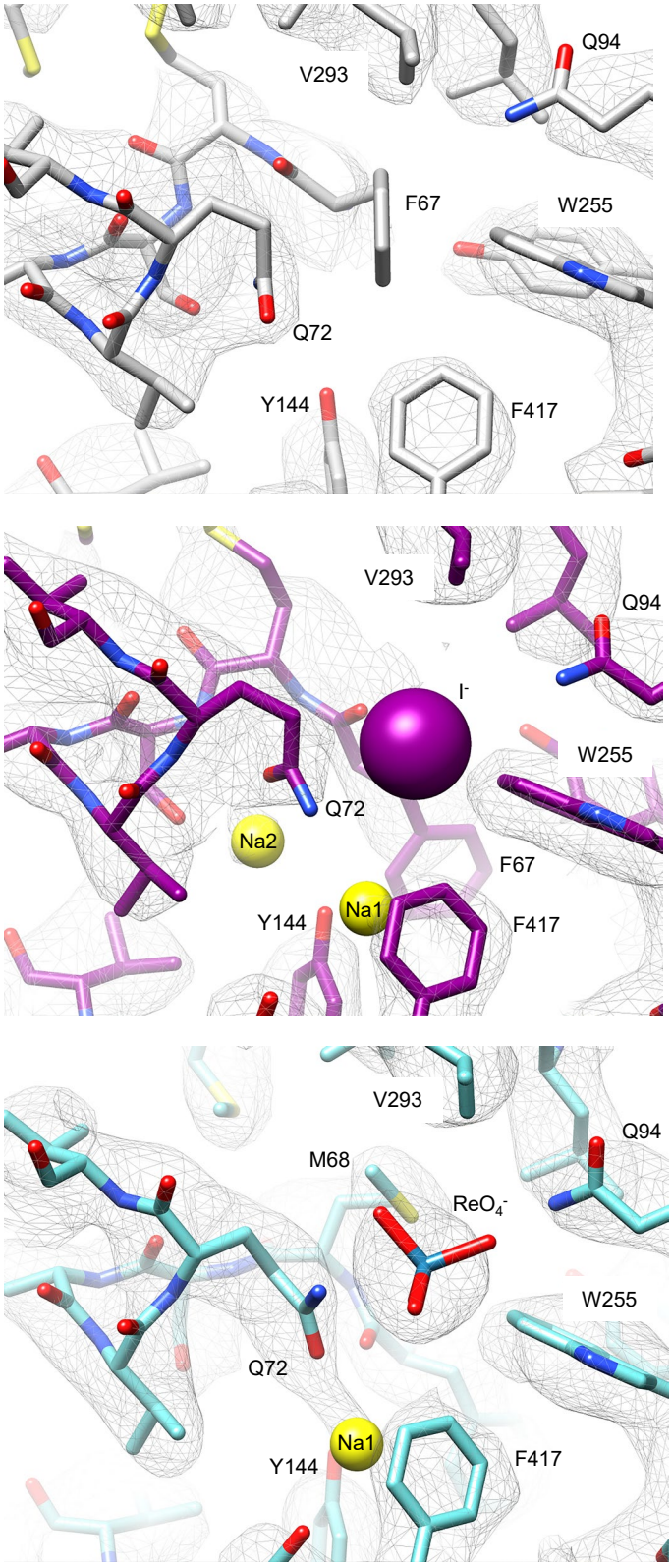

Supplementary Fig. 10 Local densities in the Apo-NIS (top), NIS-I^- (middle), and NIS-ReO_4^- (bottom) maps show that the Q72 side chain has a different conformation in each of the three structures.

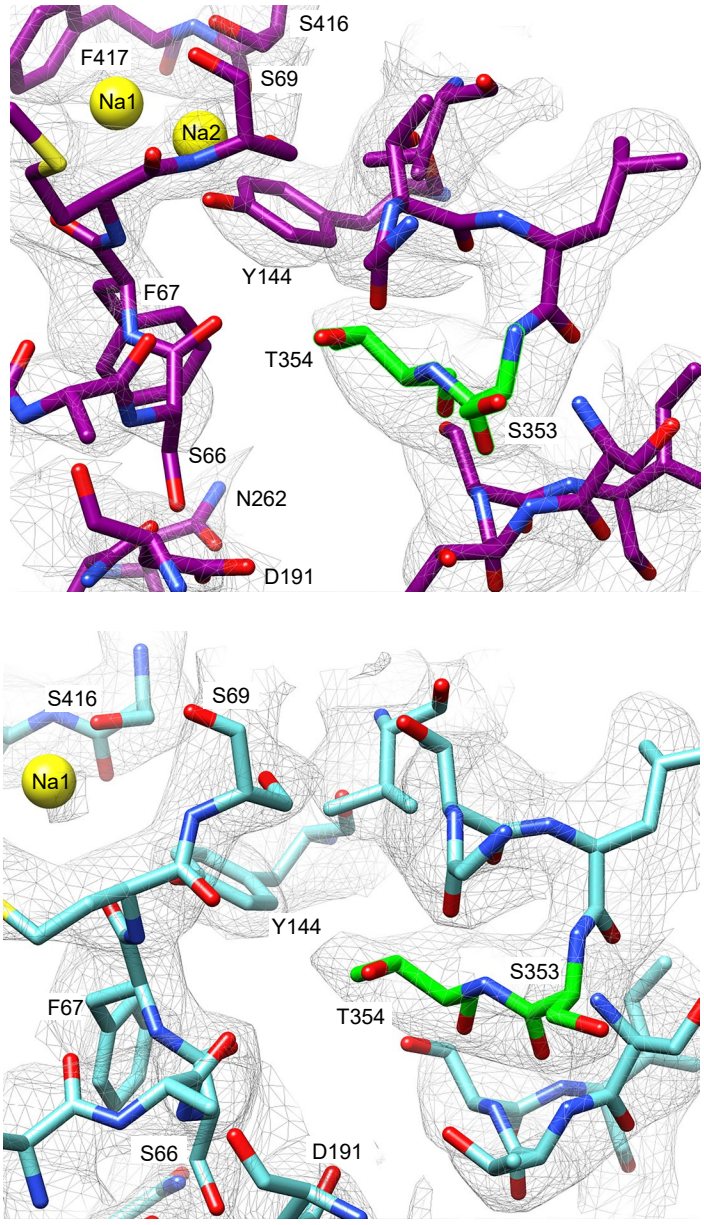

Supplementary Fig. 11 Close-up of the NIS region containing the β-hydroxyl residues that form the canonical Na2 site. S353 and T354, highlighted in green—in the NIS-I^- (top) and NIS-ReO_4^- (bottom) structures.

Supplemental Information Table S1. Composition of, and production times for, the MD simulation system.

Complex	Atoms	Lipids (DOPC)	Number of ions	Ligands	Water molecules	Simulation time
I^-/Na^+	161318	405	87 Na^+ and 92 Cl^-	2Na^+ and 1I^-	32586	5390 ns